Continuous monitoring by ambient-seismic noise tomography

Sjoerd de Ridder

ABSTRACT

Seismic arrays permanently installed over a hydrocarbon reservoir can record data continuously, even in the absence of active seismic shooting. Here we study ambient-seismic noise tomography as a tool for continuous monitoring. This is of interest for both monitoring production-related changes over a long time scale (years), but it may also be a source of data for monitoring hazards over short time scales (days to weeks). We compare cross-correlations of partial recordings to cross-correlations of the full recording as a function of absolute recording time, inter-station distance and frequency. We use straight-ray tomography to image the virtual-seismic sources for travel times picked after band passes for various frequencies. The correlations converge faster for nearby receiver pairs and lower frequencies than for further receiver pairs and higher frequencies. The convergence rate also depends on the strength of the microseism energy in the ambient seismic field. Features visible in ambient-seismic noise tomography images of Scholte wave group-velocity for various frequency bands are compared to slices of a P wave velocity cube obtained from full waveform inversion of active seismic data. Clear similarities indicate that the Scholte wave group-velocity between $0.15 - 0.75$ Hz forms an image up to a depth of 240 meters. Clear similarities indicate that the Scholte wave group-velocity between $0.15 - 0.75$ Hz forms an image up to a depth of 240 meters. This study shows the feasibility of ambient-seismic noise tomography monitoring of the near surface.

INTRODUCTION

Reservoir monitoring by active seismic is a well-established technique. A single survey provides an image of the subsurface at a given time. Repetitive seismic surveying provides differential seismic images that show how the subsurface changes over time, relative to a baseline survey. At Valhall, in the Norwegian North Sea, a permanent four component (4C) Ocean Bottom Cable (OBC) array was installed in 2003 (Kommedal et al., 2004) for repeated active seismic surveying. These conventional surveys provide subsurface images after lengthy seismic acquisition, processing, and imaging procedures, at only a few snapshots in time. The OBC array is capable of continuously recording for long periods of time in the presence or absence of active seismic shooting.

Recordings in the absence of controlled-seismic shooting are referred to as passive-seismic recordings. Their use is widespread in both global- and exploration-seismology. Passive-seismic recordings contain earthquake energy of rupture events as large as the 2004 Sumatra Earthquake, $M_w = 9.1$, (Ammon et al., 2005), and as small as hydraulic induced microseismic fracture events in reservoirs, $M = -2$, (Shemeta and Anderson, 2010). Studies of earthquakes and microseismic events are of deterministic nature, aimed at characterizing the source and its wavefield. However, even in the absence of discrete deterministic events, passive-seismic recordings contain an abundance of energy, also referred to as the Earth's Hum (Rhie and Romanowicz, 2004, 2006). These are continuous excitations of the Earth's free modes. One strong such series of excitations is the microseism energy captured in the Earth's surface interface modes. The waves in these modes are propagating randomly, as such no particular events can be distinguished. Hereafter this microseism energy will also be referred to as ambient-seismic noise.

Recordings of microseism energy can be made continuously and thus are a potential source of data for continuous reservoir monitoring. This is not only of interest for monitoring production-related changes over a long time scale, but also a possible source of data for short time scale hazard monitoring.

Passive seismic interferometry is a technique that cross-correlates ambient-seismic noise recordings at two stations to form a signal, the estimated Green's function (EGF), as if one of the stations was a seismic source (Wapenaar and Fokkema, 2006). Virtual seismic Scholte wave sources have previously been used in tomographic studies of the near surface (Bussat and Kugler, 2009; de Ridder and Dellinger, 2011). This technique allows for the design and installation of a system that exploits the ambient-seismic noise field to perform continuous, nearly real-time reservoir surveillance. The reliability of retrieved subsurface information depends on the characteristics of the ambient seismic field and its excitation sources. We need to investigate how much ambient-seismic noise is needed to cross-correlate for the retrieve of stable EGFs and reliable tomographic images.

This paper is outlined as follows. In the first section we briefly review passive seismic interferometry. Then we explore the ambient seismic microseism energy at Valhall and its capability to create low frequency virtual seismic sources. In the following section we elaborate on the filtering and correlation procedures. We then explore with how much data the correlations convergence towards the long-term correlation average. The next section contains straigth-ray tomography results at various frequency bands and for correlations of various portions of the data. The paper finishes with a discussion and some concluding remarks.

PASSIVE SEISMIC INTERFEROMETRY

To perform passive seismic interferometry, we cross-correlate passive seismic recordings between all possible station pairs in a permanently installed array. This creates

a full virtual seismic survey, $\mathbf{D}(\omega) = \mathrm{D}(\omega, x_r, x_s)$:

$$\mathbf{D}(\omega) = \mathbf{r}(\omega)\ \mathbf{r}(\omega)^{\dagger}, \tag{1}$$

where $\mathbf{r}(\omega) = \mathrm{r}(\omega, x)$ is a vector containing passive seismic recordings at all stations, and † denotes the Hermitian (complex conjugation and transposition). However, this technique holds only when the energy in the ambient seismic field satisfies a condition known as energy equipartitioning. In practice, this requirement limits the application of seismic interferometry to certain frequency regimes. The ambient seismic field at low frequencies (0.18 - 1.75 Hz) is dominated by the double-frequency microseism peak, a source of seismic energy that satisfies the requirement of energy equipartition and can be utilized for seismic interferometry (Stewart, 2006; Dellinger and Yu, 2009). At the Valhall oil field, this microseism energy is recorded by the aforementioned permanent installed seismic array (see station map in Figure 1). The microseism energy recorded by the vertical component of the OBC consists of excitations of the Scholte-wave mode of the seafloor.

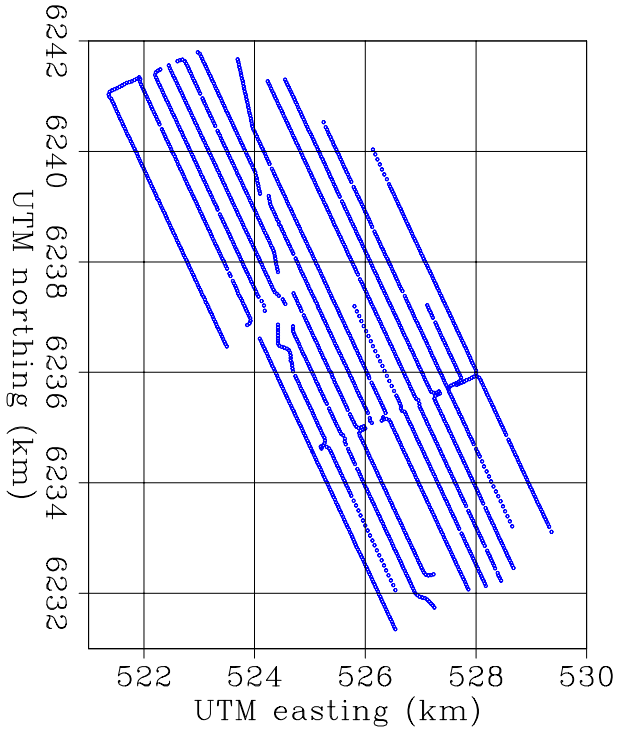

Figure 1: Station map of OCB at Valhall. [**ER**]

These installations are capable of making recordings continuously for long periods and under all weather conditions. One such recording was made in December 2010, spanning a little over 5 days. Figure 2 shows how the spectrum of the ambient seismic field, as recorded far away from the platform, changes over time. The spectrum is computed over 2.5 minute overlapping windows and averaged over several receivers far removed from the platform. Clearly the microseism energy strength varies over time. Figure 3 contains recordings of wave height and wind strength made at Ekofisk (NMI, 2012), another oil-field near Valhall. Although the weather station is at 32 km from

Valhall, there is a clear correlation between the strength of the microseism energy and the wind strength. This corroborates atmosphere-ocean-seafloor coupling as the source of this microseism energy (Longuet-Higgins, 1950; Rhie and Romanowicz, 2004, 2006). An example of a virtual source is shown in Figure 4. This is one column

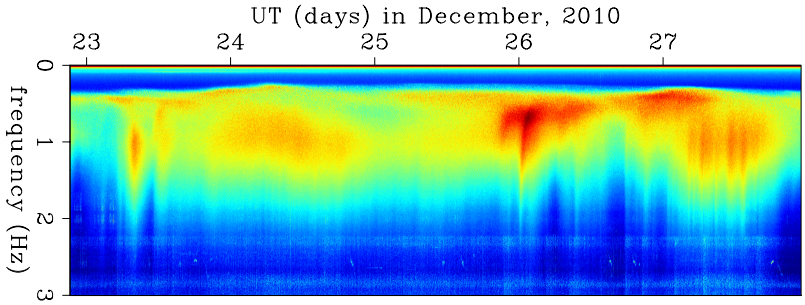

Figure 2: Spectrum of the ambient seismic field, computed over 2.5 minute overlapping windows. The spectrum is averaged over several receivers far removed from the platform and displayed as a function of time. [**CR**]

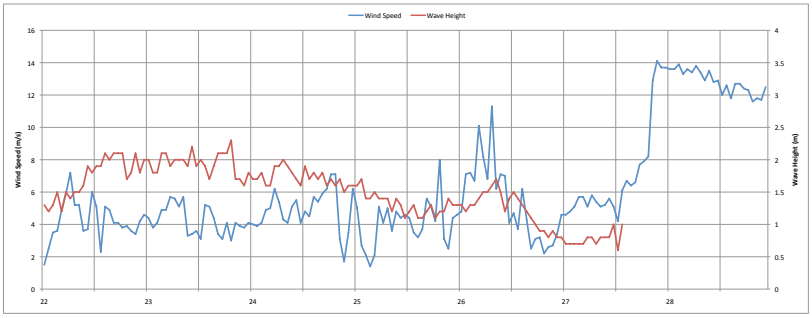

Figure 3: Wind-speed and wave-height measurements at Ekofisk, another oil field near the Valhall field (NMI, 2012). [**NR**]

in the matrix $\mathbf{D}$, for which all data are cross-correlated with the data at a station in the center of the array. Six time slices are shown, at 0, 3, 6, 9, 12 and 15 seconds. Although the energy focuses at the source at $t = 0$ seconds, there is energy at $t = 0$ in the vicinity of the master station because the virtual source is finite in bandwidth and zero phase. The wavefront is dispersive: lower frequencies propagate faster the higher frequencies. The virtual source radiates very homogeneously in all directions, reflecting that the energy in the ambient seismic field, averaged over 5 days, was travelling in about equal strength in all directions. The dispersion in the virtual sources can be made visible by transforming the virtual sources from the (t, x) domain to the (ω, p) domain and stacking all virtual sources in one line of the Valhall array together. The dispersion image is shown in Figure 5. For most of the frequency range, the virtual sources are dominated by a single dispersive wave mode.

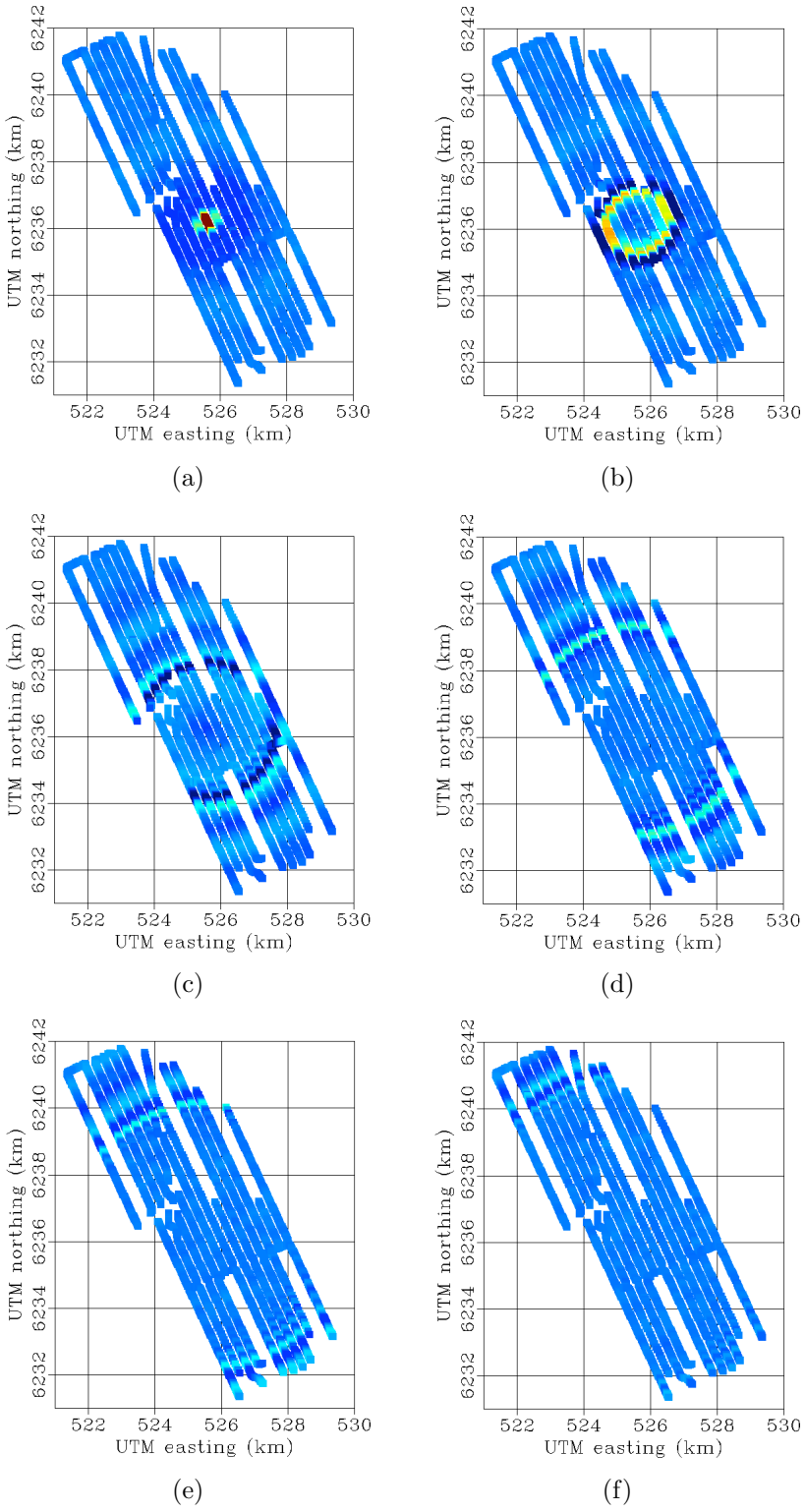

Figure 4: A virtual seismic source located in the center of the array. Time slices at: 0 (a), 3 (b), 6 (c), 9 (d), 12 (e) and 15 seconds (f). [**NR**]

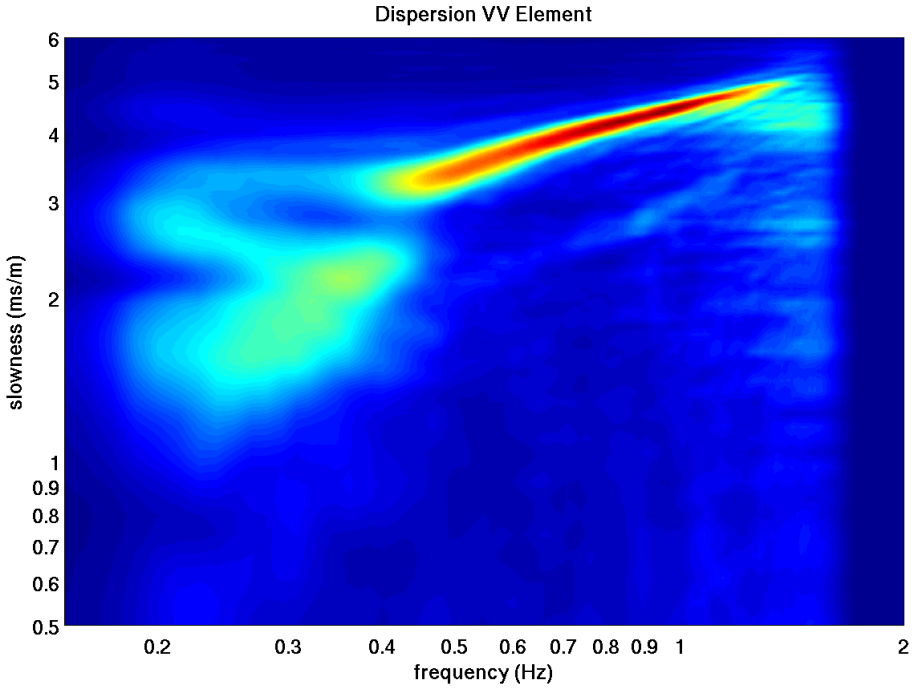

Figure 5: Dispersion image for virtual seismic sources in one OBC line of the array. The virtual sources are dominated by a single, dispersive wave mode. [**NR**]

FILTERING AND CORRELATION PROCEDURES

These data were recorded by stations designed for active seismic surveying. It was made available with a sampling frequency of 500 Hz, which is common for active seismic data. However, these long and continuous recordings are not perfect; they are contaminated with data glitches, electronic noise, and other noise bursts. It is best to deal with these imperfections before any further processing, because they can cause strong filtering artefacts. The next step is to bandpass the data for the frequency range of interest ($0.18 - 1.75$ Hz), which is considerably lower than the frequency range of active seismic imaging. For recordings at Valhall, this part of the frequency spectrum is fairly clean (see Figure 2), especially far from the platforms.

These data are divided into blocks of 30 minutes with 50% overlap between adjacent blocks and multiplied with a cosine-squared taper. This taper has the advantage of restitching the data together without amplification, according to the Pythagorean trigonometric identity. Each 30 minute block is bandpassed (for $0.18 - 1.75$ Hz) and subsampled by a factor of 50 to a sample frequency of 10 Hz. The data is not restitched, instead, the 30 minutes of data are cross-correlated between each station pair, delivering one EGF for each station pair. For all data in the December 2010 recording, this gives 486 EGFs for each station pair.

Figure 6a) shows one such estimate for all stations cross-correlated with station 1, Figure 6b) shows the mean of all estimates for 2 hours, Figure 6c) shows the mean of

all estimates for 1 day, and Figure 6 shows the mean of all estimates for a little over 5 days. In each individual estimate there is little signal that exceeds the background correlation fluctuations. However, as we stack more estimates and thus increase the effective recording time we cross-correlate, over arrivals start standing out from the background correlation fluctuations. These arrivals correspond to the surface-wave Green's function between all stations and station 1.

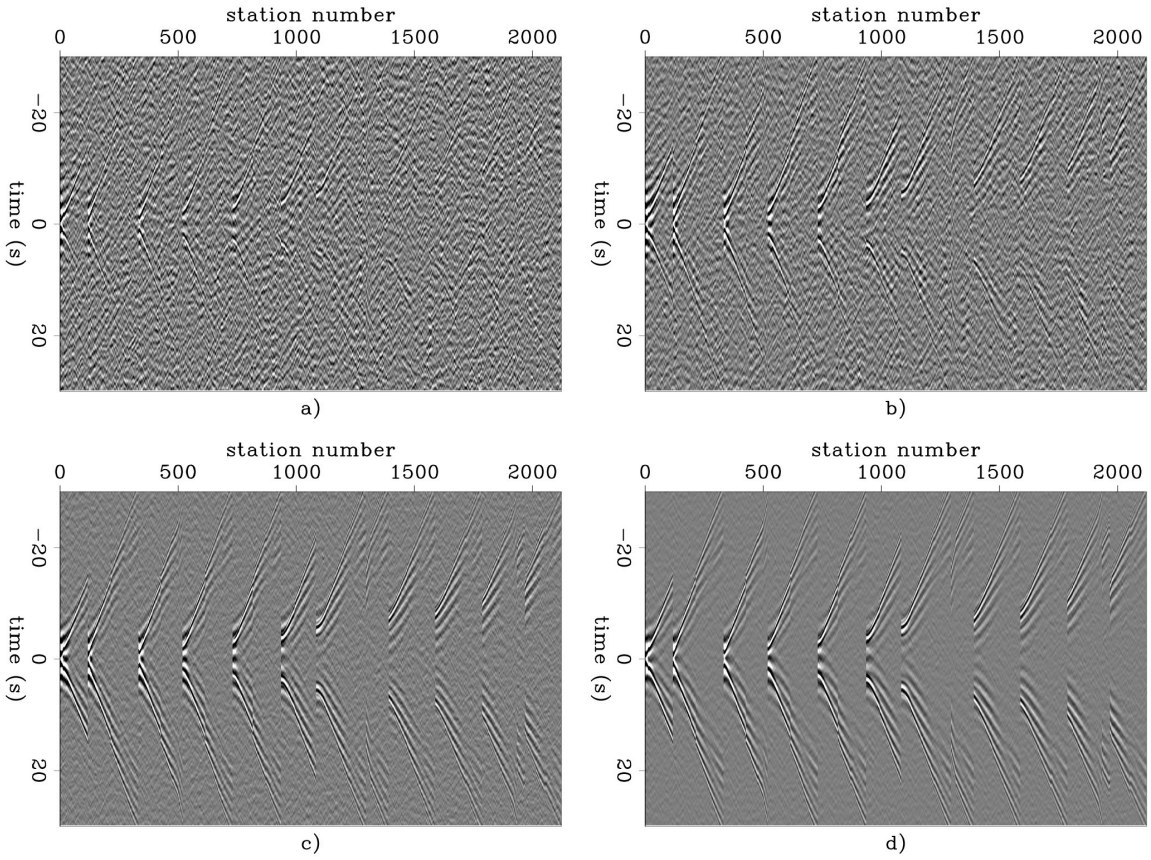

Figure 6: Four virtual seismic sources generated by cross correlating recordings of ambient seismic noise; a) 1/2 hour of recordings, b) 2 hours of recording, c) 1 day of recording, d) 5 days of recording. [**CR**]

CONVERGENCE RATE OF AMBIENT-SEISMIC NOISE CORRELATIONS

To design an installation that exploits seismic interferometry as a permanent, continuous, nearly real-time monitoring system, we need to investigate how much ambient-seismic noise we must cross-correlate to retrieve a stable EGF. The correlation coefficient between two virtual sources, one created by correlating 3 hours of data and one created by correlating all data, as a function of the center-time of the shorter recording. A high correlation coefficient means that the correlation of the partial recording

is very similar to a correlation of the full signal. This analysis should be made with caution, because there is no measure of the physical correctness of the EGF in these correlation coefficients. Theoretically, the inclusion of more time in longer records could deteriorate the correlation signal as an estimation of the Green's functions. However, the comparison of correlations of a partial recording with the total recording gives a measure of the convergence rate and the stability of the estimated Green's function. The resulting correlation coefficients are averaged for a virtual source in the center of the array and a source at the north-west end of the array, as shown in Figure 7. These measures for correlation-convergence show similarity with the strengths of the microseism energy as seen in Figure 2, but the especially strong periods of microseism energy on the 26^{th} and 27^{th} of December are less dominant in Figure 7. When higher frequencies are particularly strong, the partial stack does not resemble the full stack very well.

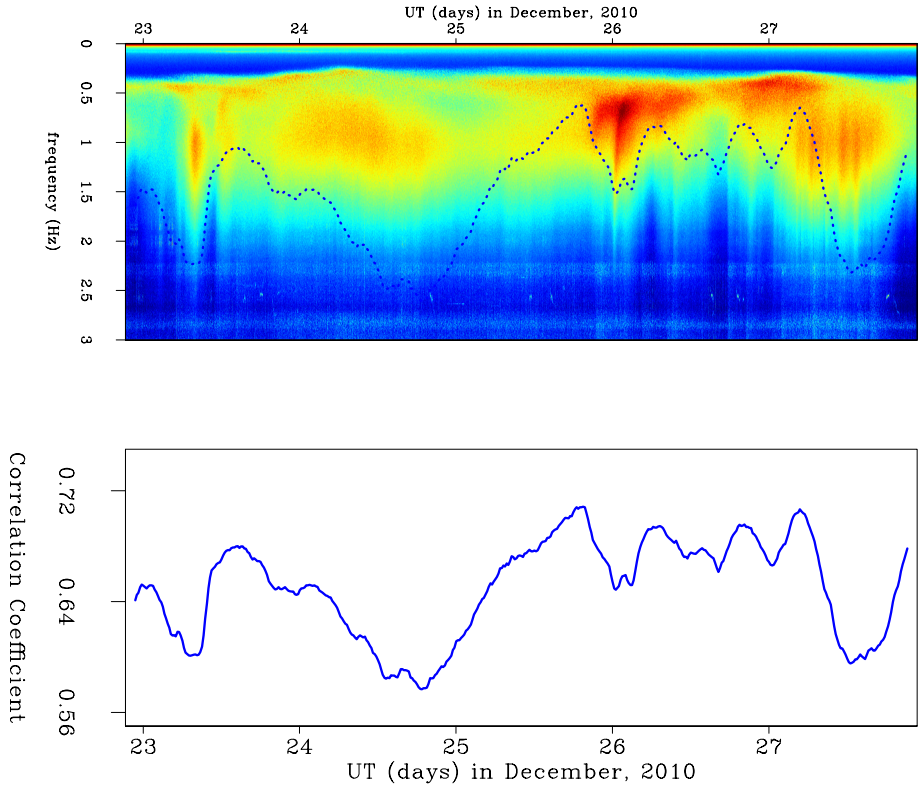

Figure 7: Correlation coefficients as a function of start time comparing a 3 hour partial window with the full stack. The top panel shows the spectragram with the correlation coefficients overlayed and the bottom panel shows only the curve of correlation coefficients. [**CR**]

We want to analyse the cross-correlation convergence rate as a function of inter-station distance for various frequency ranges. We compute the correlation coefficient between two virtual sources after bandpassing for a certain central frequency, and bin the coefficients as a function of inter-station distance. One virtual sources is com-

puted by cross-correlating all data while the second is computed cross-correlating a partial recording. Furthermore, to eliminate sensitivity to a particular starting time of the partial recording, we slid the partial recording window across the complete recording. We repeat the whole procedure for two virtual sources and average the mean correlation coefficients for each distance bin and partial recording length. The frequency range $1.50 - 1.75$ Hz is shown in 8a, $1.50 - 1.75$ Hz in 8b, $1.25 - 1.50$ Hz in 8c, $1.00 - 1.25$ Hz in 8d, $0.75 - 1.00$ Hz in 8e, $0.50 - 0.75$ Hz in 8f, $0.25 - 0.50$ Hz in 8f. Dotted and dashed lines are 0.50 and 0.95 contours. The contour lines are not very smooth. This can probably be improved by averaging the computations for more virtual sources. These figures show a trend of faster convergence rate for lower frequencies. This trend is especially apparent with inter-station distances larger than 1000 meters. This trend is expected, because low frequencies have a larger Fresnel zone than do higher frequencies, and therefore require fewer sources surrounding the stations. Since the same sources excite the entire frequency regime, the background correlation fluctuations will be dominated by higher frequencies, and the correlation will stabilize faster for lower frequencies. Correlations between stations at shorter distances converge much faster, but a trend for different frequencies at shorter distances is not clear. This behavior explains the results in Figure 7, where a strong presence of high frequencies actually deteriorates the convergence rate.

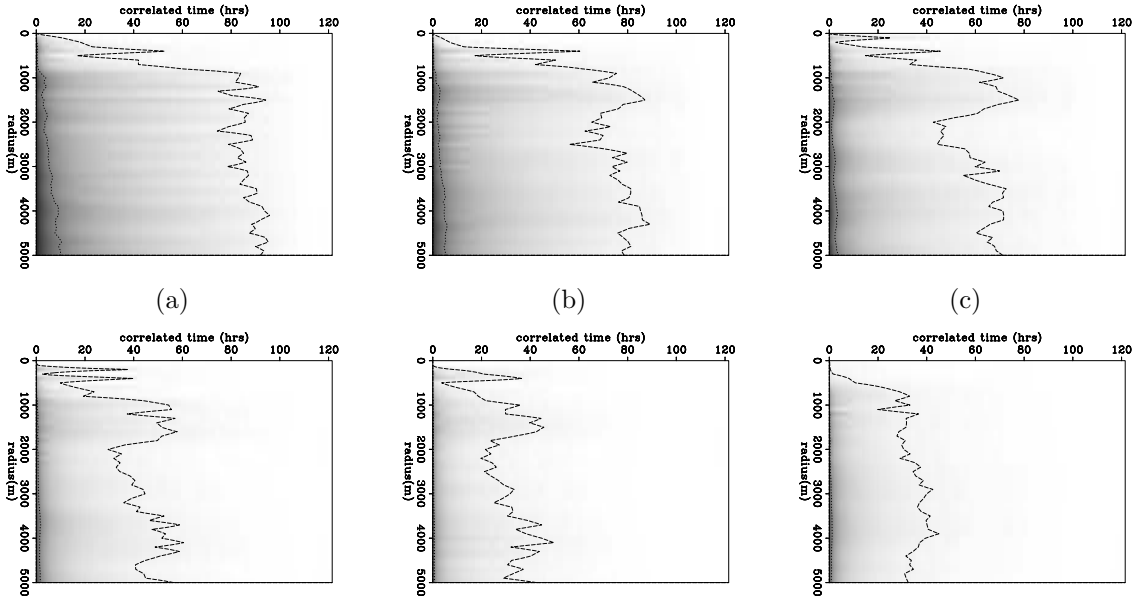

Figure 8: Correlation coefficient of partial versus total cross-correlated signal time. Dotted and dashed lines are 0.50 and 0.95 contours. Analysis made for frequency ranges; $1.50-1.75$ Hz in (a), $1.50-1.75$ Hz in (b), $1.25-1.50$ Hz in (c), $1.00-1.25$ Hz in (d), $0.75 - 1.00$ Hz in (e), $0.50 - 0.75$ Hz in (f), $0.25 - 0.50$ Hz in (f). [**CR**]

AMBIENT SEISMIC-SEISMIC NOISE TOMOGRAPHY

The virtual seismic sources are dominated by dispersive surface waves. These propagate in two dimensions along the seafloor through a frequency-dependent velocity map. Group velocities of the surface waves can be found for narrow frequency ranges. We use a simple Hann-window bandpass to select a narrow frequency range, and then we pick travel times by the maximum of the envelope of the filtered time-domain virtual-source arrival. We define a quality factor on each pick by a signal to noise ratio (SNR): the maximum of the envelope within a linear moveout window to the average of the envelope outside the window. For various narrow frequency bands we selected travel times, $\mathbf{t}$, with an SNR > 5 and at offsets between 50 and 1750 meters. These travel-time picks were input into a straight-ray tomography kernel, linearized with perturbations, $\Delta\mathbf{m}$, in an average velocity, m_0:

$$\mathbf{m} = \mathrm{m}_0 + \Delta\mathbf{m}, \tag{2}$$

$$\mathrm{m}_0 = \frac{1}{N}\sum_{i=1}^{N}\frac{\mathbf{t}}{\Delta\mathbf{x}}, \tag{3}$$

$$\Delta\mathbf{t} = \mathbf{t} - \mathrm{m}_0\,\Delta\mathbf{x}, \tag{4}$$

where $\Delta\mathbf{t}$ are the travel-time residuals after accounting for the contribution of the average velocity and $\Delta\mathbf{x}$ is the offsets for each specific travel-time pick. The tomography-problem fitting goals are posed as follows:

$$\mathbf{F}\Delta\mathbf{m} - \Delta\mathbf{t} = \mathbf{0}, \tag{5}$$

$$\epsilon\nabla^2\Delta\mathbf{m} = \mathbf{0}, \tag{6}$$

where we use the ∇^2 operator as regularization to force a smooth model, and the total model is reconstructed by summing with the background velocity.

The aim is to create group-velocity maps at different frequencies by picking a group travel time at the peak of the envelope after a narrow-range bandpass. Lower-frequency group-velocity maps should reflect deeper structures, because at lower frequencies (and thus longer wavelengths), surface waves are sensitive to deeper structures. Picking a frequency range that is too narrow would result in an oscillatory wavelet and make travel-time picks less accurate. Figure 9 contains a set of inversion results using virtual sources of different frequency ranges. Six overlapping frequency ranges were selected: $0.15 - 0.75$ Hz, $0.35 - 0.95$ Hz, $0.55 - 1.15$ Hz, $0.75 - 1.35$ Hz, $0.95 - 1.55$ Hz and for $1.15 - 1.75$ Hz. At all ranges but the lowest, the wave-mode is very sharply defined in the dispersion image of Figure 5.

Stacking just one day of data gives five independent stacks. Five tomographic images, one for each day, of group-velocity for the frequency range $0.75 - 1.35$ Hz are shown in Figure 10. And five tomographic images, one for each day, of group-velocity for the frequency range $1.15 - 1.75$ Hz are shown in Figure 11. Stacking two and a half day of data gives two independent stacks. Four tomographic images, of both

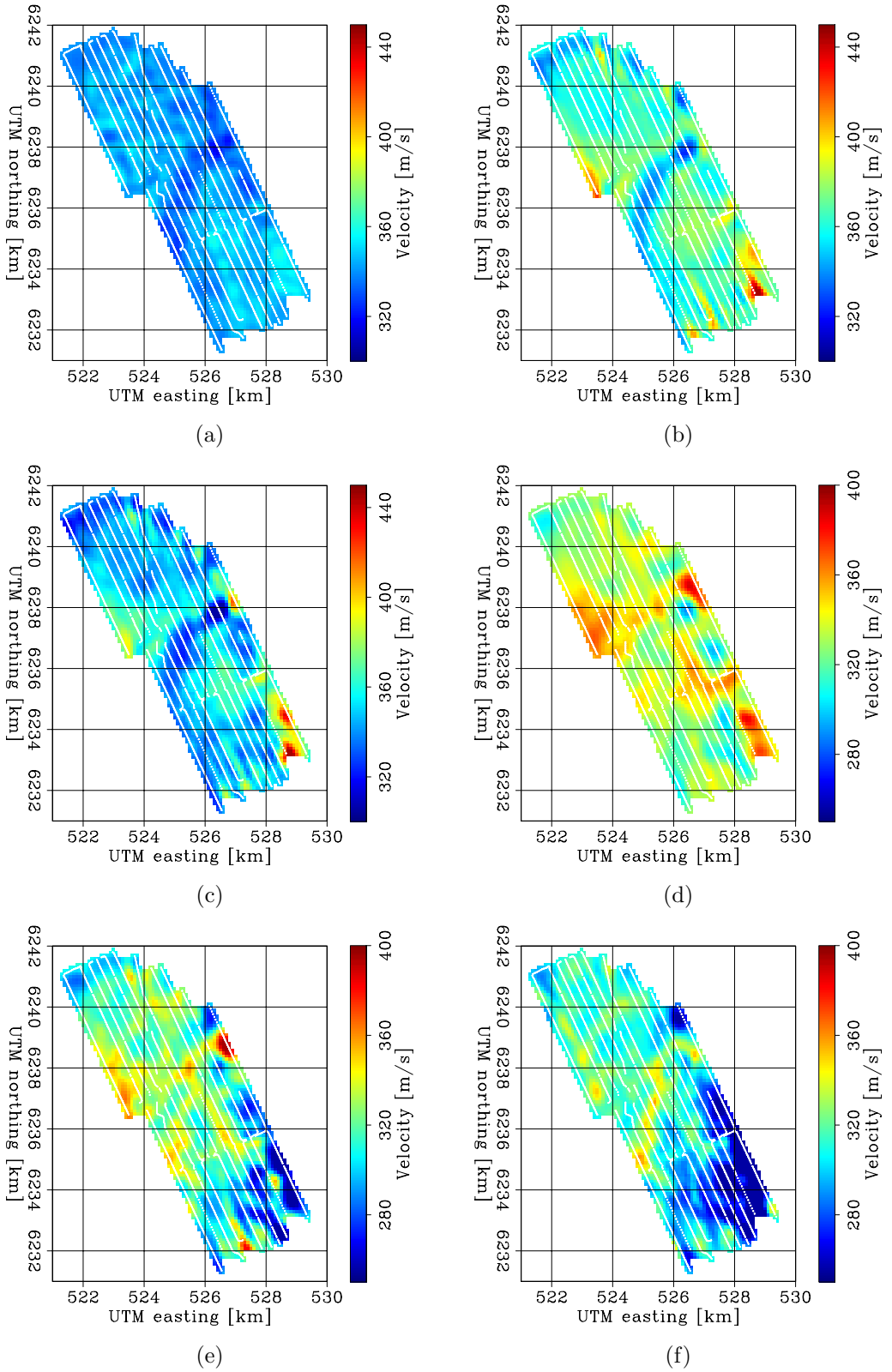

Figure 9: Tomography results for various frequency bands: $0.15-0.75$ Hz (a), $0.35-0.95$ Hz (b), $0.55-1.15$ Hz (c), $0.75-1.35$ Hz (d), $0.95-1.55$ Hz (e), and for $1.15-1.75$ Hz (f). [**CR**]

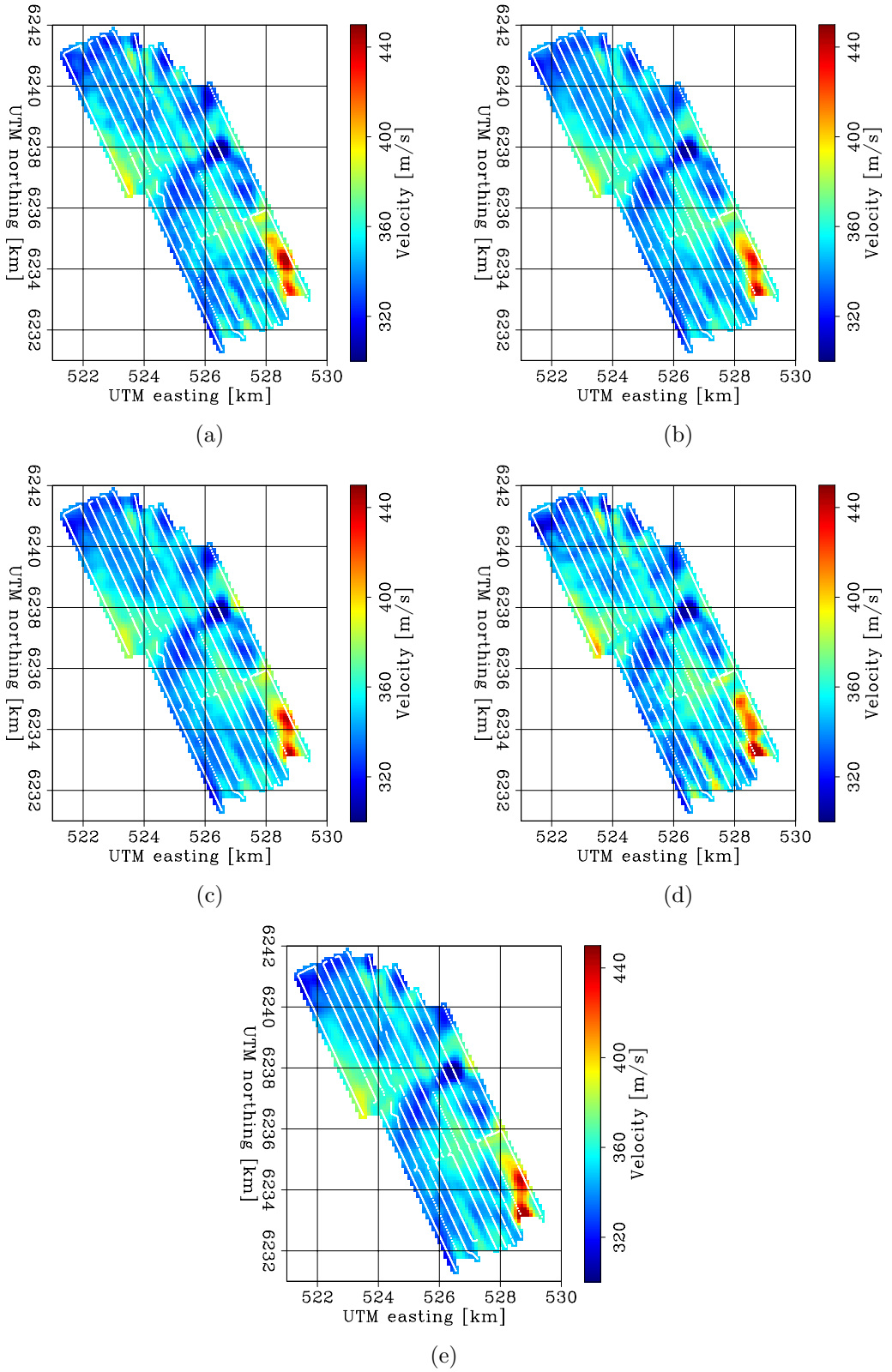

Figure 10: Tomographic results for correlations of one day of data between 0.75 – 1.35 Hz: day 1 (a), day 2 (b), day 3 (c), day 4 (d), day 5 (e). [**CR**]

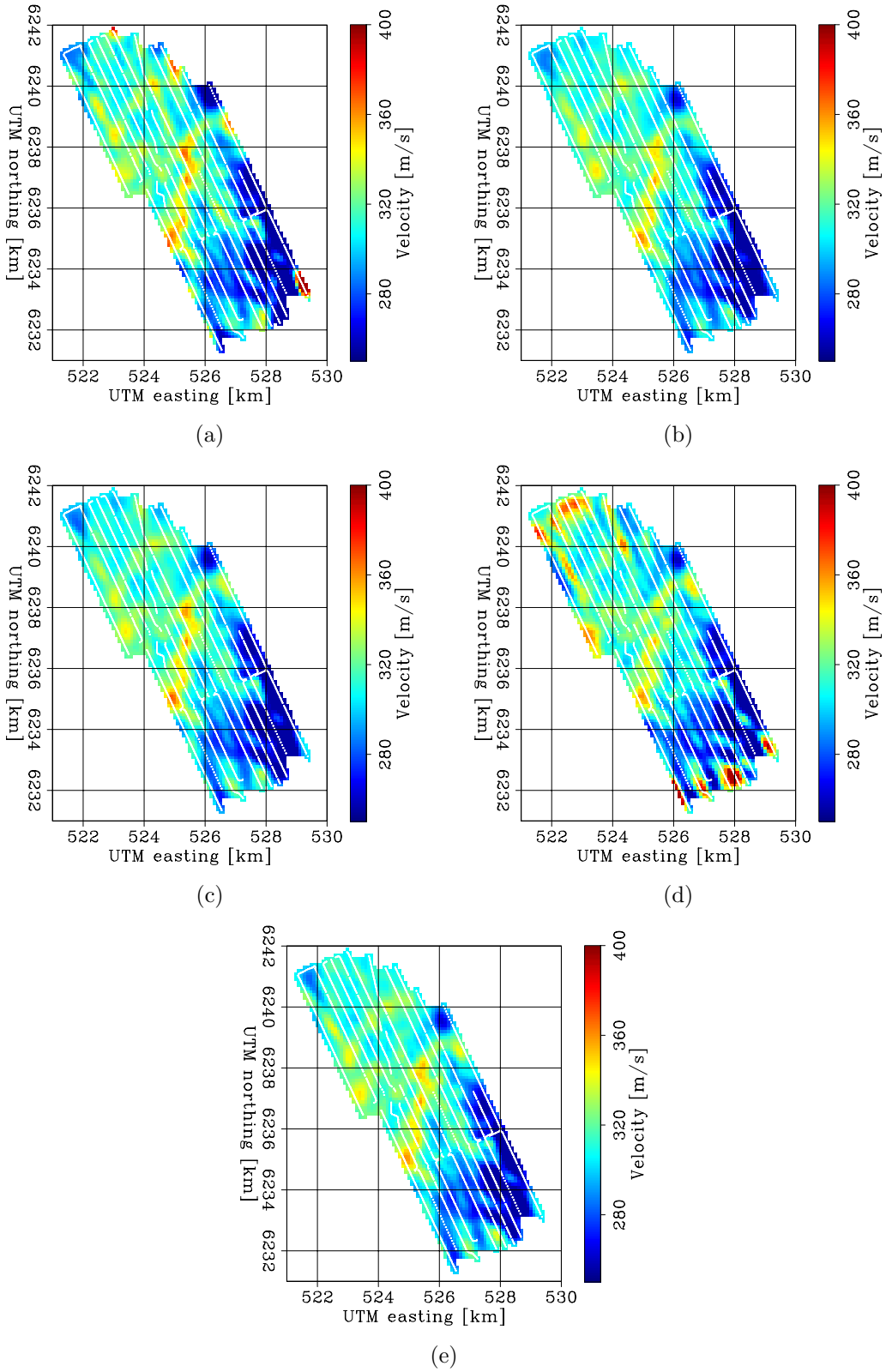

Figure 11: Tomographic results for correlations of one day of data between 1.15 – 1.75 Hz: day 1 (a), day 2 (b), day 3 (c), day 4 (d), day 5 (e). [**CR**]

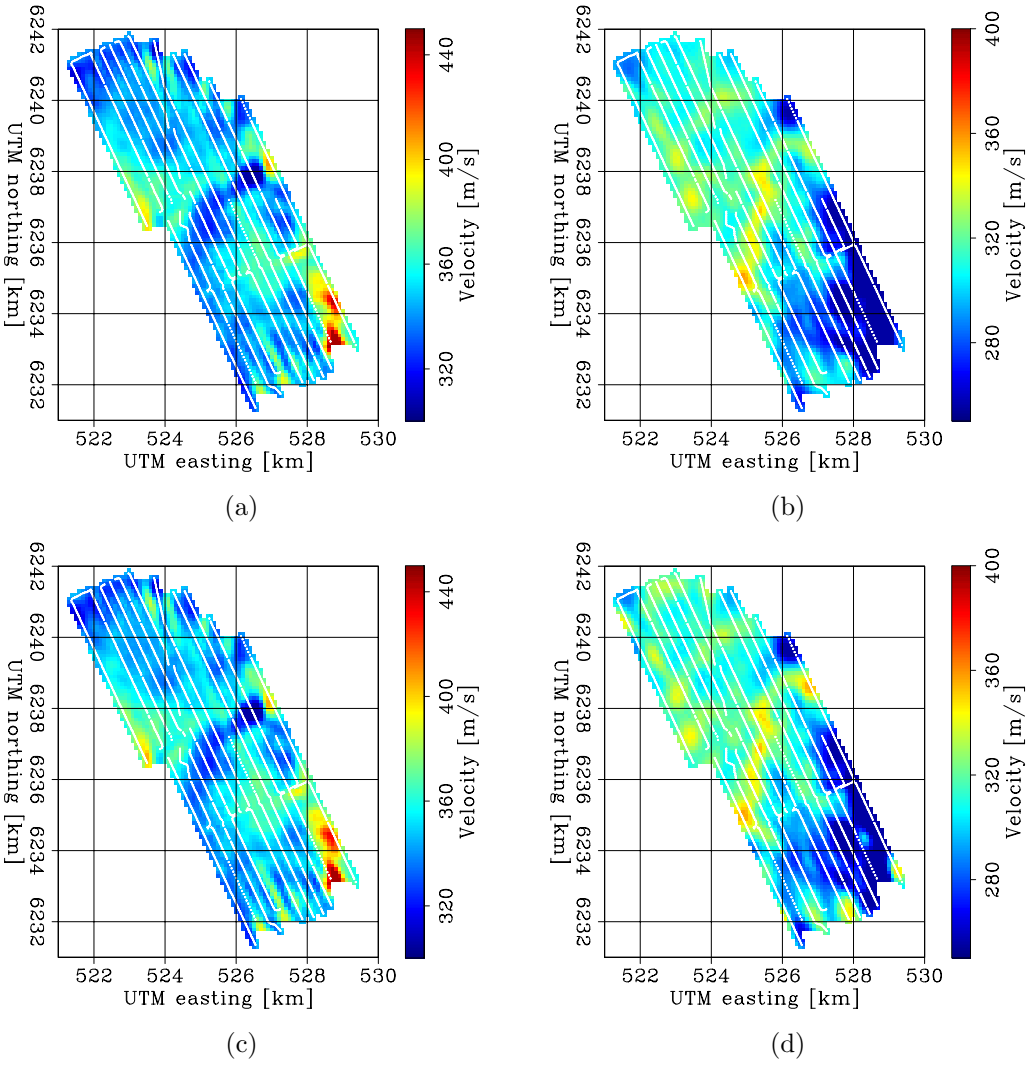

Figure 12: Tomographic results for correlations of two and a half days of data between $0.75 - 1.35$ Hz (a) and (c) and for correlations between $1.15 - 1.75$ Hz: from the first two and a half days in (a) and (b), from the second two and a half days in (b) and (d). [**CR**]

stacks, of group-velocity for the frequency ranges $0.75 - 1.35$ Hz and $1.15 - 1.75$ Hz are shown in Figure 12. These tomographic images are similar but not the same.

We can compare these group-velocity images to P-wave velocity images obtained by full wave-form inversion of active seismic surveys (Sirgue et al., 2010). These images include features extending beyond the extent of the receiver array, because the active sources cover a wider area than the receivers do. Whereas the maps obtained from ambient-seismic noise tomography are logically confined within the area of the recording array. In the 240 meters below the seafloor, the P-wave velocity maps show several buried channels as high-velocity anomalies. The bigger channel on the east is as deep as 105 to 240 meters. There are smaller channels buried in the top 100 meters. Below one of the smaller shallow channels is a low-velocity zone that crosses the array; this feature is apparent between 150 and 240 meters.

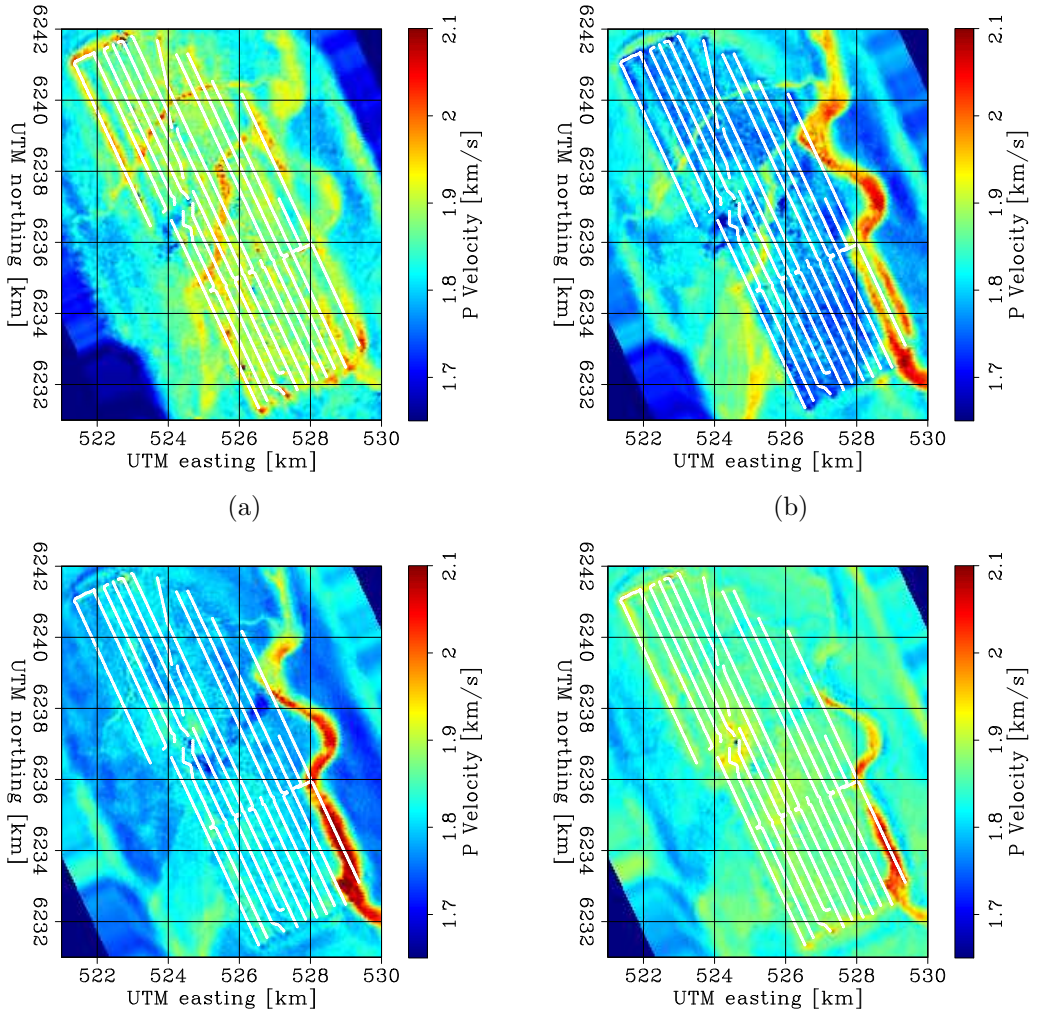

Figure 13: Image of P-wave velocities obtained using wave-form inversion of active P-wave data (Sirgue et al., 2010). Velocity slices are for the following depth ranges: $60 - 105$ m (a), $105 - 150$ m (b), $150 - 195$ m (c), and $195 - 240$ m (d). [**NR**]

DISCUSSION AND CONCLUSIONS

Previous passive seismic interferometry studies have used tomography to image the surface wave Green's functions for reservoir studies (Bussat and Kugler, 2009; de Ridder and Dellinger, 2011). Here we investigate the utilization of passive seismic interferometry as a permanent, continuous, nearly real-time monitoring system. The correlations stabilize faster for lower frequencies than for higher frequencies. We show that correlations of as little as 1 day of data between nearby receivers for frequencies below 1 Hz converges to 95% of the correlation of 5 days of data. The group-velocity maps obtained from ambient-seismic noise tomography contain similar features in different frequency regimes. The smaller shallow channels are visible between $0.95 - 1.75$ Hz. The edge of the deeper channel is visible on the southeastern end of the array between $0.35 - 1.35$ Hz. A low-velocity zone crosses the array and is clearly distinguishable between $0.35 - 1.15$ Hz. The images are generally smoother than the P-wave velocity images from ambient-seismic noise tomography. This is partly because of the smoothing of the velocity map, but since the frequency of the ambient-seismic noise is also lower than that of active seismic surveying, the resolution cannot be expected to be as high. The very nature of the seismic waves used for the imaging is different. Surface waves propagate along the surface, and thus the depth resolution is provided only by their dispersive characteristics and cannot be expected to be as high as for P-waves. Nevertheless, we can achieve remarkable images of the top 240 meters based on Scholte-wave velocities obtained by ambient-seismic noise correlations. These are of interest for continuous reservoir monitoring, especially for short time scale (days) changes in the shallow subsurface. The similarity of tomographic images obtained from independent day long cross-correlations or even two-and-a-half long cross-correlations needs further quantification.

ACKNOWLEDGEMENTS

Thanks to Joe Dellinger and Olav Barkved of BP for discussions, suggestions and support of this study and for comments on this work. Thanks to Biondo Biondi, Bob Clapp and Jesse Lawrence for helpful discussions and suggestions. And thanks to BP and the partners of the Valhall Field (BP Norge A/S and Hess Norge A/S) for the data.

REFERENCES

Ammon, C. J., C. Ji, H.-K. Thio, D. Robinson, S. Ni, V. Hjorleifsdottir, H. Kanamori, T. Lay, S. Das, D. Helmberger, G. Ichinose, J. Polet, and D. Wald, 2005, Rupture process of the 2004 Sumatra-Andaman earthquake: Science, **308**, 1133–1139.

Bussat, S. and S. Kugler, 2009, Recording noise - estimating shear-wave velocities: Feasibility of offshore ambient-noise surface-wave tomography (answt) on a reservoir scale: SEG Technical Program Expanded Abstracts, **28**, 1627–1631.

de Ridder, S. and J. Dellinger, 2011, Ambient seismic noise eikonal tomography for near-surface imaging at Valhall: The Leading Edge, **30**, 506–512.

Dellinger, J. A. and J. Yu, 2009, Low-frequency virtual point-source interferometry using conventional sensors: 71st Meeting, European Associated of Geoscientists and Engineers, Expanded Abstracts, Expanded Abstracts, X047.

Kommedal, J. H., O. I. Barkved, and D. J. Howe, 2004, Initial experience operating a permanent 4C seabed array for reservoir monitoring at Valhall: SEG Technical Program Expanded Abstracts, **23**, 2239–2242.

Longuet-Higgins, M. S., 1950, A theory of the origin of microseisms: Philosophical Transaction Royal Society Londen A, **243**, 135.

NMI, 2012, Norwegian Meteorological Institute climate data database: http://sharki.oslo.dnmi.no/. (last visited: March 1, 2012).

Rhie, J. and B. Romanowicz, 2004, Excitation of earth's continuous free oscillations by atmosphere-ocean-seafloor coupling: Nature, **431**, 552–556.

———, 2006, A study of the relation between ocean storms and the Earths hum: Geochem. Geophys. Geosyst., **7**, Q10004.

Shemeta, J. and P. Anderson, 2010, It's a matter of size: Magnitude and moment estimates for microseismic data: The Leading Edge, **29**, 296–302.

Sirgue, L., O. I. Barkved, J. Dellinger, J. E. U. Albertin, and J. H. Kommedal, 2010, Full waveform inversion: the next leap forward in imaging at Valhall: First Break, **28**, 65–70.

Stewart, P., 2006, Interferometric imaging of ocean bottom noise: SEG Technical Program Expanded Abstracts, **25**, 1555–1559.

Wapenaar, K. and J. Fokkema, 2006, Green's function representations for seismic interferometry: Geophysics, **71**, SI33–SI46.

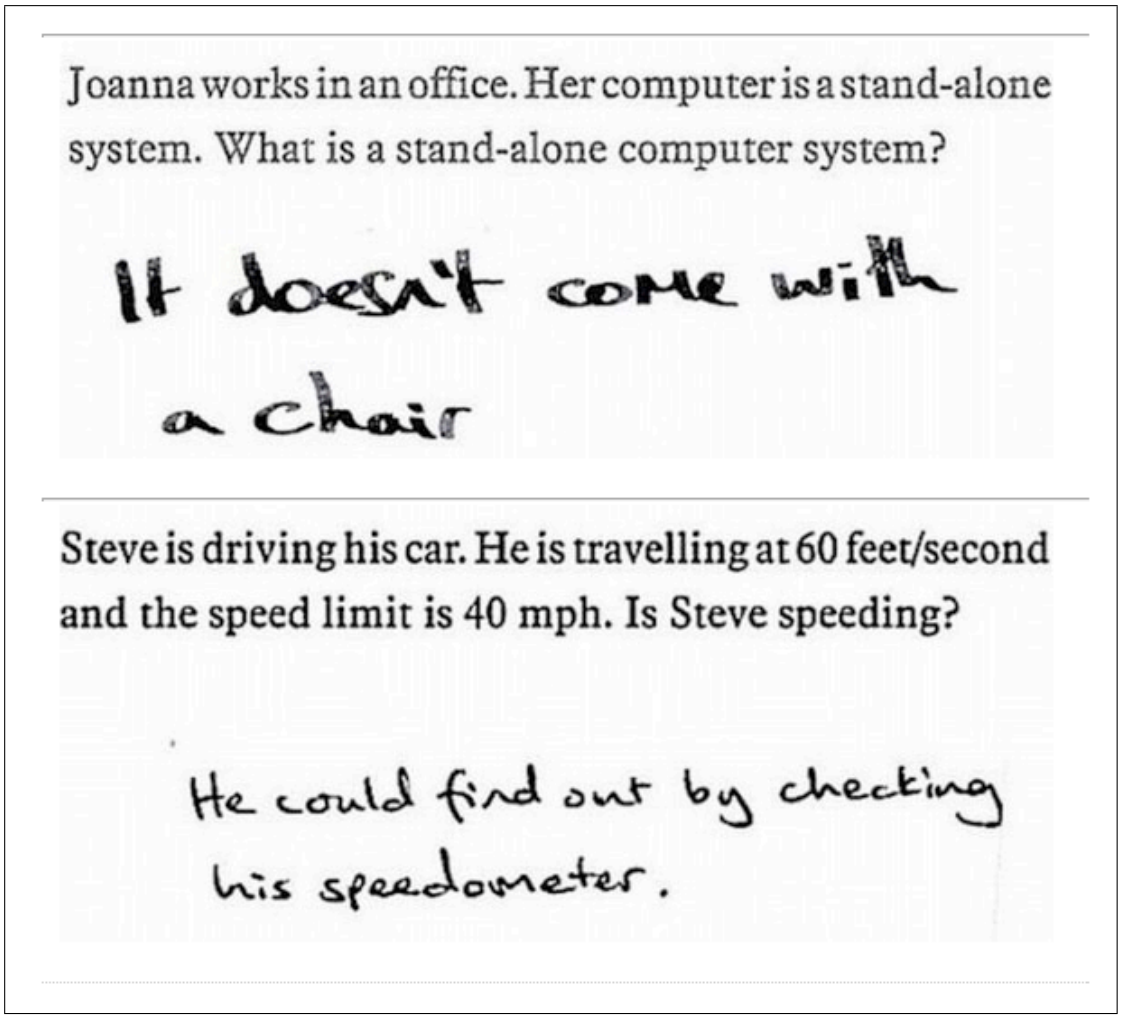
Joanna works in an office. Her computer is a stand-alone system. What is a stand-alone computer system?
It doesn't come with a chair
Steve is driving his car. He is travelling at 60 feet/second and the speed limit is 40 mph. Is Steve speeding?
He could find out by checking his speedometer.